Polymer Bulletin (2021) 78:2439–2463
https://doi.org/10.1007/s00289-020-03222-3

ORIGINAL PAPER

Synthesis of polyaniline/clay nanocomposites by in situ polymerization and its application for the removal of Acid Green 25 dye from wastewater

Shivani Kalotra[1] · **Rajeev Mehta**[1]

Received: 1 October 2019 / Revised: 8 March 2020 / Accepted: 27 April 2020 / Published online: 9 May 2020

Abstract

Synthesis, characterization and adsorption studies of polyaniline (PANI) and polyaniline/montmorillonite clay (PANI/MMT) nanocomposites have been carried out. In situ polymerization method was used to synthesize PANI/MMT nanocomposites using HCl as a catalyst and ammonium persulfate as an oxidizing agent. The molar ratio of monomer/oxidant was 1:1, and the polymerization was done at two different temperatures, i.e.,. 0° and 20 °C. Complete removal of Acid Green 25 (AG25) dye was achieved with PANI/MMT adsorbent. The kinetic adsorption data of AG25 dye were found to fit pseudo-second-order kinetic model. Since the removal of this dye takes place efficiently at a very fast rate, PANI/MMT nanocomposites will be excellent adsorbents in continuous adsorption systems.

Keywords Polyaniline · Montmorillonite clay · Nanocomposites · Adsorption · Acid Green 25 dye

Introduction

Contamination in water produced from several industries such as paper, textiles, cosmetics, pharmaceuticals, leather, plastics, printing and rubber industry is highly toxic and harmful to human beings [1, 2]. Textile industry in particular discharges a very large amount of dye bearing wastewater. There are three

Electronic supplementary material The online version of this article (https://doi.org/10.1007/s00289-020-03222-3) contains supplementary material, which is available to authorized users.

✉ Rajeev Mehta
rajeevmehta33@yahoo.com

Shivani Kalotra
shivani.kalotra@gmail.com

[1] Department of Chemical Engineering, Thapar Institute of Engineering and Technology, Patiala 147004, India

categories of dyes: anionic dyes, cationic dyes, non-ionic dyes, and most of these are toxic and some are carcinogenic [3–5]. Acid dyes are anionic dyes, and these are highly soluble in water [6]. Acid dyes are generally used in nylon, silk and wool industries [7]. AG25 is an anionic dye and used in a number of applications, including textile, cosmetic, wood, leather and paints industry [8, 9]. AG25 dye effluent is very harmful to aquatic creatures. It can cause many problems for human beings like skin and eye irritation. Therefore, it is important to eliminate AG 25 dye from textile wastewater through different treatment methods so that we can protect our environment.

Several methods are used for the adsorption of textile dyes from wastewater such as membrane separation, coagulation, flocculation, chemical oxidation, adsorption, biodegradation, electrochemical processes and ozonation [4, 10, 11]. In the present study, the focus is on the adsorption method. It is the easiest but may not be the most efficient method for reducing dye contamination [10]. Many researchers have studied the adsorption of textile dye waste using different types of adsorbents and the selection of an adsorbent depends upon its various characteristics like cost-effectiveness, easy recovery, non-toxic, easily available and regenerable [12].

Polyaniline (PANI) has been extensively studied mainly because of its unique conductivity properties. It has a great potential for industrial applications on a large scale [13]. The advantages of PANI are its easy synthesis, high electrical conductivity, low cost of raw materials, high stability [14, 15], redox properties [16], lightweight, good processability and outstanding magnetic and optical properties [17]. PANI also exhibits relatively high porosity and surface area [18] and would be a good candidate for dye removal by adsorption.

Polyaniline is synthesized from the aniline monomer either by electrochemical or chemical polymerization process [19, 20]. On a larger scale, the chemical polymerization is the most suitable technique for the synthesis of polyaniline [19]. Polyaniline is present in three oxidation states: emeraldine salt (ES)-doped state and emeraldine base (EB)-undoped state, pernigraniline base (PB) and leucoemeraldine base (LB) [21, 22]. Structure of polyaniline is presented in Fig. 1.

In the general structural form of polyaniline, the oxidation state is described by $(1-x)$ value and degree of polymerization is described by n. Leucoemeraldine base is fully reduced state and $x=1$ for this state. Emeraldine is half oxidized state and $x=0.5$ (i.e., equal number of oxidized and reduced units). Pernigraniline

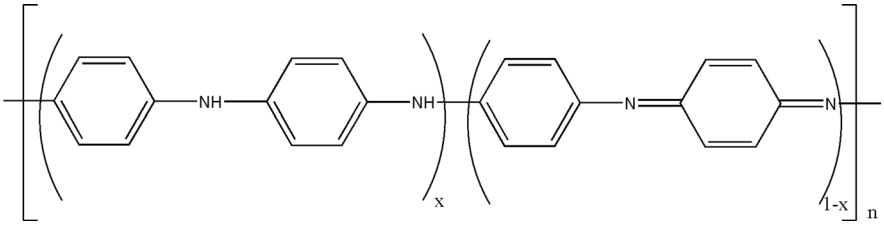

Fig. 1 Structure of polyaniline [23]

base is a fully oxidized state and $x = 0$ for this state [16, 23]. The polyaniline emeraldine salt is a dark green powder (characteristic particle size: 3–100 μm) of average density 1.36 g/mL and is soluble in various common organic solvents.

PANI synthesis has been researched a lot in the literature, but the optimization of the polymerization conditions has been related to PANI applications as a conductive polymer. A review of PANI polymerization and PANI/clay in situ nanocomposites [15, 17–19, 21–56] is given in the supplementary data in Table S1a, b.

A polymer nanocomposite (PCN) is a material with vastly improved properties as compared to the individual polymers. The PCN has been synthesized for most polymers of importance [57]. The filler used in the study is a nanoclay. The clay particles have several advantages such as low cost, large surface area, high chemical stability, ultrafine particle size, high cation exchange capacity, high adsorption capacity and ion exchange properties [34, 58].

Montmorillonite (MMT) clay having the general formula $M_x(Al_{4-x}Mg_x)Si_8O_{20}(OH)_4$ belongs to the family of 2:1 phyllosilicates (comprised of two tetrahedral and one octahedral sheet of average thickness 1 nm) [34, 59–61]. MMT is hydrophilic and should be compatible with PANI, for the synthesis of polyaniline/clay nanocomposites [34, 62].

Literature review for the treatment of wastewater with PANI and PANI/clay nanocomposites [3, 4, 14, 18, 21, 58, 63–74] is given as supplementary data in Table S2.

The present study focuses on the in situ polymerization synthesis and characterization of PANI and PANI/clay nanocomposite beads for their use as an adsorbent. Adsorption behavior has been investigated using Acid Green 25 dye (AG25) as the adsorbate.

Experimental

Materials

Aniline (ACS reagent, ≥ 9.5% purity) (IUPAC name: Penylamine), hydrogen chloride (HCl), ammonium persulfate (AR, ≥ 98.5% purity) (chemical formula: $(NH_4)_2S_2O_8$) (IUPAC name: diazanium; sulfonatooxy sulfate) and montmorillonite (chemical formula: $(Na,Ca)_{0.33}(Al,Mg)_2(Si_4O_{10})(OH)_2{\cdot}NH_2O$)) clay were purchased from the company Sigma-Aldrich (India). Acetone (2-propanone) and NMP (1-methyl-2-pyrrolidone) were purchased from LOBA Chemicals.

The Acid Green 25 (anionic dye, CI. No.61570, molecular weight: 622.58 g/mol) was also purchased from the company Sigma-Aldrich, India. The chemical formula of Acid Green 25 dye is $C_{28}H_{20}N_2Na_2O_8S_2$, and absorption peak λ_{max} is 642 nm. Its structure is shown in Fig. 2.

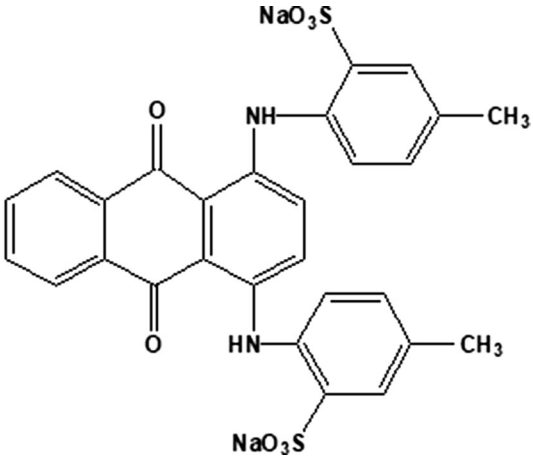

Fig. 2 Structure of Acid Green 25 (AG25) dye [68]

Method for preparation of polyaniline and polyaniline/montmorillonite clay nanocomposites and their characterization

Synthesis of PANI and PANI/MMT

PANI and PANI/MMT clay nanocomposites were synthesized at two different temperatures of 0 and 20 °C. The methodology and schematic diagram for formation of PANI/MMT nanocomposites is presented in Fig. 3.

The PANI/MMT nanocomposites were synthesized according to the experimental procedure described in the literature [38, 49], with some modifications. For the synthesis of PANI/MMT clay nanocomposites, MMT clay (0, 1, 1.5 and 2 w/v%) was dispersed in distilled water (100 ml) and sonicated for 10 min using an ultrasonicator probe to achieve clay nanodispersion. After the dispersion of the MMT clay, magnetic stirring was used to prepare PANI/MMT nanocomposites. A solution of 2 ml aniline in 1 M HCl was added slowly to the above MMT clay suspension over a period of 5 min, with magnetic stirring and the mixture was further stirred for another 20 min at 0 °C. Five grams of ammonium persulfate (oxidizing agent APS dissolved in 1 M HCl) was added slowly over a period of 10 min to the above suspension. For polymerization at 0 °C, the suspension was stirred continuously for 4 h at 0 °C to ensure the completion of the reaction. After the polymerization process, a dark green color precipitate of PANI/MMT clay nanocomposite was obtained. This product was obtained by using vacuum filtration, and it was washed with 1 M HCl, distilled water and acetone to remove ammonium persulfate and all other impurities. The obtained solid nanocomposite material was dried overnight under vacuum at 50 °C.

For the polymerization done at 20 °C, the mixture was continuously stirred at 20 °C for 2 h and the reaction for the synthesis of nanocomposite was continued for 24 h without agitation to complete the polymerization.

The same procedure was adopted to prepare polyaniline (PANI), but herein MMT clay was not added.

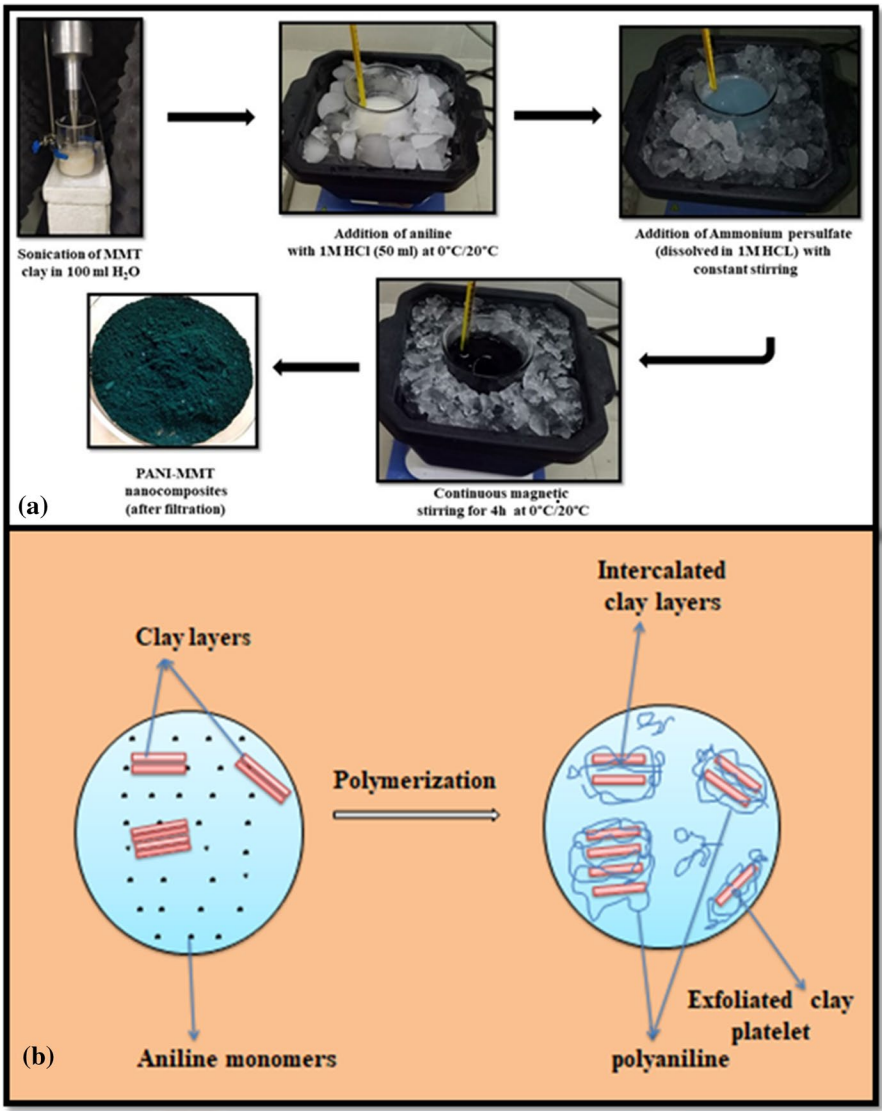

Fig. 3 **a** Methodology and **b** schematic diagram depicting the in situ polymerization preparation PANI/MMT nanocomposites

Characterization

Characterization of PANI–MMT clay nanocomposites was done by Fourier transform infrared spectroscopy, scanning electron microscopy, field emission scanning electron microscopy, X-ray diffraction, BET (Brunauer–Emmett–Teller) analysis, UV–Vis spectroscopy and HRTEM (high-resolution transmission electron microscope) technique.

The Fourier transform infrared spectra of the prepared nanocomposites were determined by PerkinElmer Spectrum RX1 using KBr pellets with the scanning range 4000–450 cm^{-1}. FTIR was used to obtain the specific bands of the prepared sample of nanocomposite. The X-ray diffractometer (XRD) was done using PanAlytical XPERT-PRO (Netherland) with a wavelength of 1.541 A° (operated at 40 mA, 45 kV). The XRD patterns were used to identify the interlayer spacing of MMT clay in nanocomposites samples. Scanning electron microscopy was recorded using an instrument JEOL (JSM-6510 LV) to determine the surface morphology of the prepared samples. The field emission scanning electron microscopy was performed using Hitachi (HI-0876-0003). A high-resolution transmission electron microscope (HRTEM) was performed using JEOL (JEM 2100 Plus). HRTEM technique is generally used to identify the nanocomposite structure more clearly. BET analysis was done to find the surface area and the pore size distribution of the samples. The equipment used for BET analysis was Microtec Belsorp Mini–II (Japan). UV–Vis spectra were recorded using PerkinElmer UV WinLab by taking the samples of PANI and PANI/MMT nanocomposites in NMP (*N*-methyl-2-pyrrolidone) solvent.

Results and discussion

Polymerization experiments

A number of experiments were performed at 0 °C and 20 °C by using ammonium persulfate as an oxidizing agent. We have selected the lower temperatures (0 °C) for adsorption experimental study, and one of the criteria adopted for the selection of temperature was lower polymerization time. Thus, PANI and PANI/MMT nanocomposites synthesized at 0 °C were selected as adsorbents for adsorption experiments of AG25 dye. The nanoclay concentration w/v (%) was varied from 0, 1, 1.5 and 2.0.

Characterization

Fourier transform infrared (FTIR) spectroscopic analysis

All the functional groups have been identified by the FTIR spectroscopy. Figure 4a, b shows the FTIR of PANI, MMT and PANI/MMT nanocomposites with various clay contents, synthesized at lower and higher temperature of 0 °C and 20 °C. The FTIR spectrum of pure MMT clay shows peaks at 3621 cm^{-1} and 3411 cm^{-1} (O–H stretching), 1016 cm^{-1} and 1101 cm^{-1} (Si–O stretching), the peak at 1633 cm^{-1} (H–O–H bending, 917 cm^{-1} (Al–OH bending), 701 cm^{-1} (Al–Mg–OH stretching), 534 cm^{-1} and 472 cm^{-1} (bands due to Si–O–Al and Si–O–Si bending). These bands have also been reported by other researchers [49, 52, 70, 75, 76, 77]. The adsorption bands of 0 °C PANI located at 1556 cm^{-1} and 1485 cm^{-1} can be attributed to the C=C stretching of the quinoid and benzenoid ring structure, respectively [34, 50, 78]. The characteristic peak of PANI at 1303 cm^{-1} is due to the C–N bending [34, 50]. The band at 1144 cm^{-1} is attributed to the formation of $^{+}HN=Q=NH^{+}$

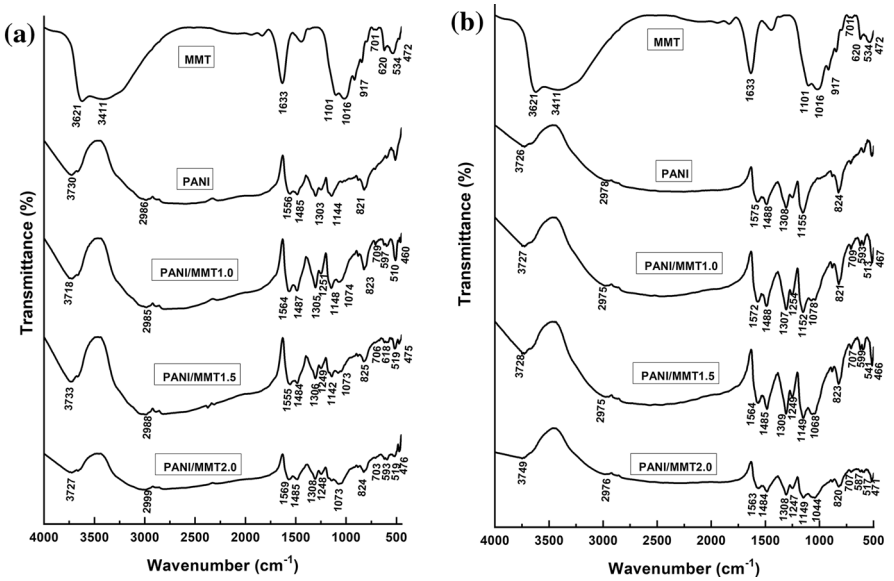

Fig. 4 FTIR spectra of MMT, PANI, PANI/MMT1.0, PANI/MMT1.5 and PANI/MMT2.0 prepared at **a** 0 °C and **b** 20 °C

structure [50]. The characteristic bands of PANI and MMT clay can be seen in the spectra of PANI/MMT clay nanocomposites in both cases (prepared at either 0 °C or 20 °C temperature with varying amount of MMT clay). The FTIR spectra of 0 °C and 20 °C are almost identical with a very small shift of peaks, and the peak intensity of 0 °C spectra is higher as compared to 20 °C spectra of nanocomposite samples. The FTIR spectra of 20 °C prepared samples are shown in Fig. 4b.

In PANI/MMT spectra, the Si–O band of MMT at 1016 and 1101 cm^{-1} gives a confirmation for the successful intercalation of PANI into the MMT clay galleries [49, 79]. However, intercalation of MMT platelet was confirmed by WAXS and HRTEM studies, as described in the following section. The Fourier spectroscopy confirms the interaction of the MMT clay layers with the PANI chains.

X-ray diffraction (XRD)

The XRD characterization was carried out to determine the insertion of PANI chains into the MMT clay interlayer space. XRD analysis was done in the 2Θ range of 3° to 70°. The XRD patterns of MMT clay and the products (PANI and PANI/MMT) prepared by in situ polymerization at 0, 1, 1.5 and 2.0 w/v (%) clay loadings are presented in Fig. 5. The PANI synthesized at 0 °C exhibited sharp peaks at $2\Theta = 25.23^{\circ}$, and two more peaks were observed at 20.94°, 14.9° and that indicates its crystalline nature [48, 80]**.** PANI prepared at 20 °C shows diffraction peaks at $2\Theta = 14.70°$, 20.41°, 25.58°, which shows the crystalline structure of the PANI [38, 44, 48, 81, 82]. Thus, the XRD spectrum of PANI obtained at 0 °C

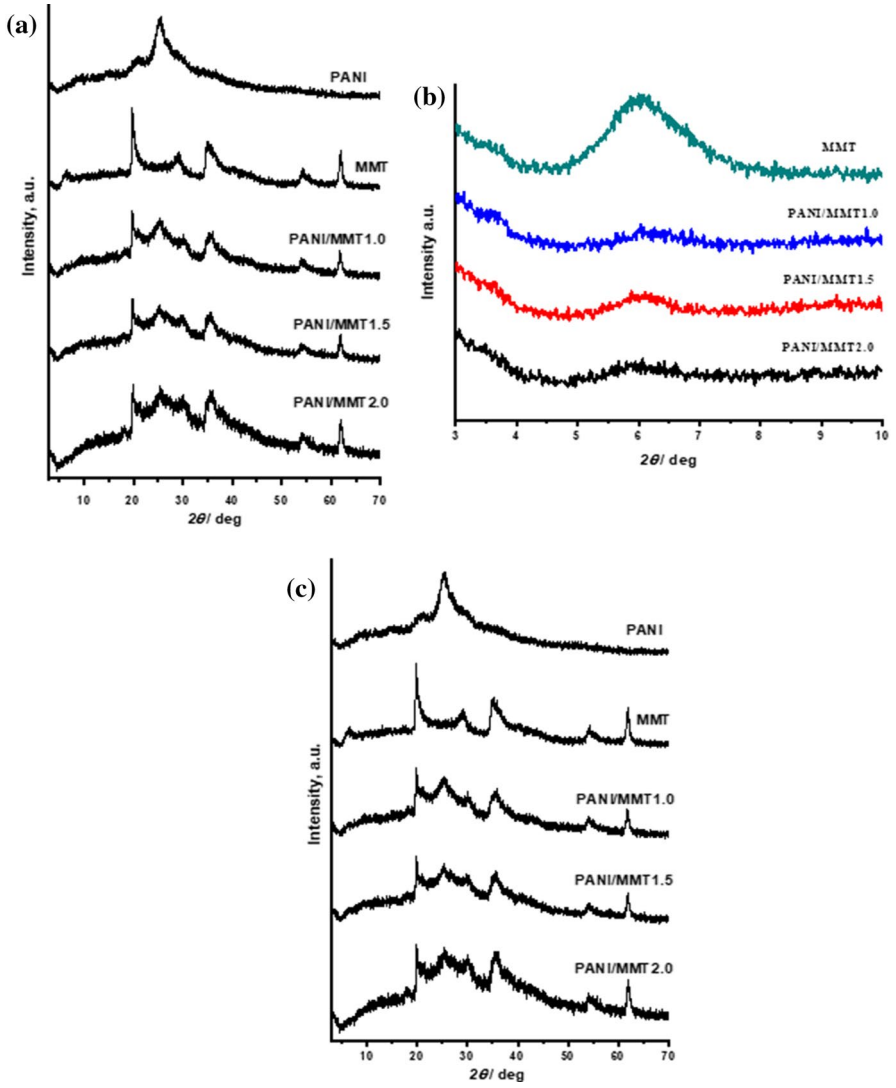

Fig. 5 **a** Wide angle and **b** Expanded angle XRD patterns of PANI, MMT and its nanocomposites prepared at 0 °C, **c** XRD pattern of PANI and nanocomposites prepared at 20 °C

and 20 °C shows similar peaks. The spectrum of pure MMT showed a d_{001} peak at $2\Theta = 6.08^{\circ}$ corresponding to d-spacing of 14.52 A°. Wide and expanded angle XRD patterns of PANI, MMT and PANI/MMT clay nanocomposites synthesized at 0 °C are shown in Fig. 5a, b. The values for PANI/MMT nanocomposites are presented in Table 1. All the samples of nanocomposites are intercalated and not exfoliated. Similar XRD results are obtained for 20 °C nanocomposite samples (Fig. 5c), and the values for 20 °C samples are presented in Table 2.

Table 1 XRD data of MMT and PANI/MMT nanocomposites prepared at 0 °C

Component	2Θ	d_{001} spacing (A°)
MMT	6.08	14.52
PANI/MMT1.0	6.28	14.05
PANI/MMT1.5	6.01	14.67
PANI/MMT2.0	5.97	14.78

Table 2 XRD pattern of MMT and PANI/MMT nanocomposites prepared at 20 °C

Component	2Θ	d_{001} spacing (A°)
MMT	6.08	14.52
PANI/MMT1.0	6.27	14.08
PANI/MMT1.5	6.09	14.50
PANI/MMT2.0	5.98	14.75

Scanning electron microscopic (SEM) analysis

The morphology of PANI (emeraldine salt) and PANI/MMT nanocomposites was studied through SEM analysis. The SEM images of pure MMT clay showed a layered structure. The morphology of the pure PANI sample synthesized at 0 °C and 20 °C confirms that the prepared PANI has a granular texture, but the morphology of PANI/MMT nanocomposites was not clearly seen in SEM analysis for both temperatures (0 °C and 20 °C), so FESEM analysis was used.

The FESEM images of pure PANI and PANI/MMT nanocomposites with 1 w/v (%) clay prepared at 0 °C and 20 °C are shown in Fig. 6. The granular structure of PANI is identified in Fig. 6a, c. There is a significance difference of morphology in PANI and PANI/MMT nanocomposites (for both 0 °C and 20 °C temperature). In Fig. 6b, d, it can be clearly seen that the polymerization mainly occurred between the clay layers. Figure 6b is the FESEM image of PANI/MMT nanocomposites prepared at 0 °C, and Fig. 6d shows the FESEM image of PANI/MMT nanocomposites prepared at 20 °C.

High-resolution transmission electron microscope (HRTEM)

HRTEM analysis was used to identify the internal structure of PANI/MMT nanocomposite. HRTEM gives more clarity about the structure. Figure 7a, b shows the HRTEM images of PANI/MMT nanocomposites synthesized by in situ polymerization at 0° and 20 °C. The clay platelets are represented by black lines, and polymer matrix is represented by gray/white surface. The HRTEM photographs of nanocomposites show that the nanocomposites consist of silicate layer and these MMT silicate layers are intercalated within the PANI matrix. HRTEM analysis confirms the intercalated structure of PANI/MMT nanocomposites.

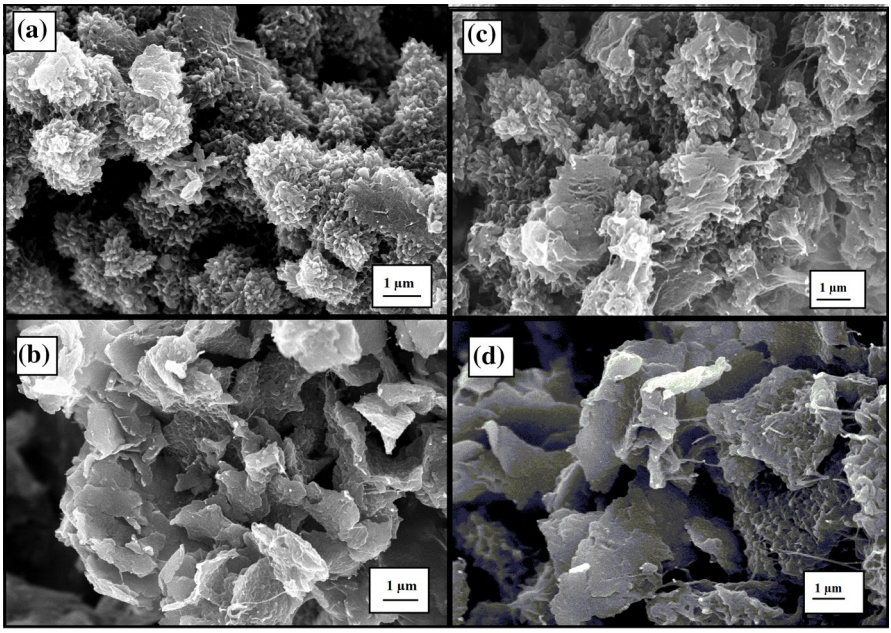

Fig. 6 FESEM images of **a** PANI and **b** PANI/MMT nanocomposites prepared at 0 °C, **c** PANI and **d** PANI/MMT samples prepared at 20 °C

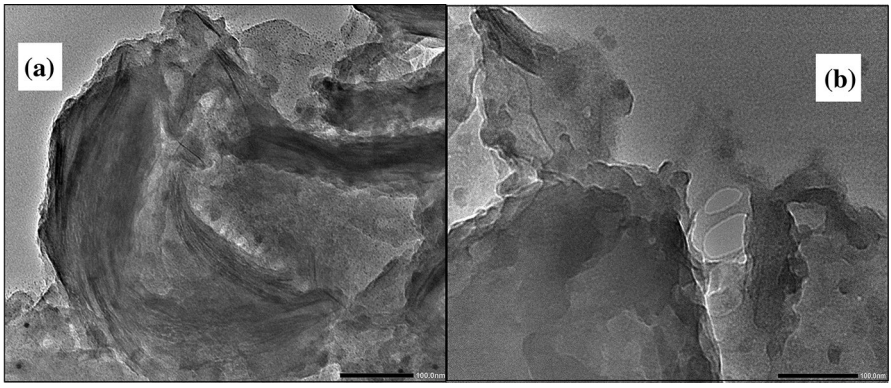

Fig. 7 HRTEM images of PANI/MMT nanocomposites

Brunauer–Emmett–Teller (BET) analysis

The surface area and pore size of pure PANI and PANI/clay nanocomposites were analyzed by BET analysis and are summarized in Table 3. Then, PANI affords a porous morphology. MMT clay morphology is less porous and has less specific surface area as found out from BET measurements as given in Table 3. However, the

Table 3 Specific surface area of PANI and its nanocomposites

Samples	Pore diameter (nm)	Pore volume (cm^3/g)	BET (m^2/g)
PANI	17.55	0.12	26.32
PANI/MMT1.0	15.63	0.07	18.28

adsorption behavior of PANI/MMT is better than pure PANI. The nanocomposite surface area is lesser than that of PANI, possibly due to the presence of millions of nanodispersed clay particles that block the pores in the PANI sample. This is so because MMT platelets, when dispersed at nanolevel, possess very large surface area, and hence, PANI/MMT would use their complementary properties forming adsorption.

UV–Vis spectroscopy

The UV–Vis spectra of pure PANI and PANI–MMT clay nanocomposites synthesized at 0° and 20 °C are displayed in Fig. 8. All the samples were dissolved in N-methyl 2-pyrrolidone (NMP) solvent and absorption bands were analyzed by UV–Vis spectroscopy. The UV–Vis spectrum of pure PANI synthesized at 0 °C exhibits two absorption bands at around 332 nm and 638 nm wavelength, which are ascribed to π−π* transition of benzoid ring and excition transitions in the quinoid ring [30, 82–86]. These bands indicate that the PANI is in an emeraldine conducting

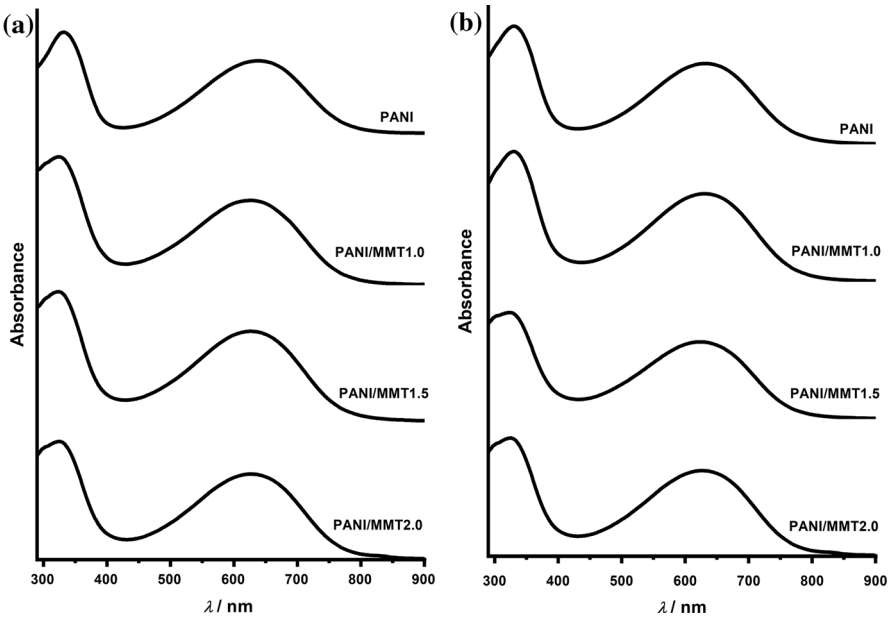

Fig. 8 UV–VIS spectra of PANI and PANI–MMT nanocomposites prepared at **a** 0 °C and **b** 20 °C

state. The characteristics absorption bands of PANI–MMT nanocomposites were found at 324 nm and 626 nm for PANI/MMT1.0; 322 nm and 628 nm for PANI/MMT1.5; and 322–326 nm and 623–628 nm for PANI/MMT2.0. The spectrum peak at 322–326 nm is assigned to π−π* transition of benzoid ring. The absorption peak at around 623–628 nm is due to the excition transition from benzenoid ring to quinoid ring [30, 85, 86]. The absorption bands of PANI and PANI–MMT nanocomposites (0, 1, 1.5, 2 w/v%) synthesized at 20 °C are very similar to those synthesized at 0 °C. For 20 °C, two bands were obtained at 331 nm and 633 nm for pure PANI that can be ascribed to π−π* transition of benzoid ring and excition transitions in the quinoid ring. The UV absorption peaks were found at 330 nm and 630 nm for PANI/MMT1.0, 324 nm and 624 nm for PANI/MMT1.5, 322–326 nm and 623–628 nm for PANI/MMT2.0. In polyaniline/MMT nanocomposites samples, the adsorption bands shifted slightly to a lower wavelength and this indicates the MMT clay and polyaniline interaction.

Method for adsorption studies

The prepared PANI and PANI nanocomposites (prepared at 0 °C) were studied for their adsorption behavior.

Adsorption studies were done by diluting a stock solution of Acid Green 25 dye (1 g/L) into different dye concentrations solutions (50–200 mg/L). The parameters studied were: effect of dye solution temperature (20 to 50 °C), adsorbent dose (0.008–0.6 g), initial dye concentration (50–200 mg/L), time (0–60 min) and pH (2–10). For the adsorption study, 100 mL of various initial dye concentration solutions was prepared along with a fixed amount of adsorbent. The experiments were carried out in an incubator shaker at 180 rpm for 60 min at pH 6 by varying temperature from 20 to 50 °C.

The percentage of dye removal was calculated by:

$$\%\text{removal} = 100\left(C_o - C_e\right)/C_o \tag{1}$$

where C_o = initial concentration of AG25 dye. C_e = equilibrium concentration (mg/L) of AG25 dye.

The equilibrium capacity of the dye was calculated by:

$$q_e = \left(C_o - C_e\right)V/m \tag{2}$$

where q_e = amount of AG25 dye adsorbed at equilibrium per unit mass of adsorbent (mg/g). V = volume (L) of AG25 dye solution. m = mass (g) of adsorbent.

The first parameter studied was pH of dye solution.

Effect of pH

The interaction between the adsorbate and the adsorbent is significantly affected by the pH of the dye solution. The chemistry of adsorbate solution, ionization degree of adsorbate molecules and the surface charge of adsorbent are strongly

affected by the pH of dye solution [66, 70]. The effect of pH on the adsorption of AG25 dye was investigated on pure PANI and PANI/MMT by varying pH values in the range of 2 to 10. The pH of the dye solution was adjusted using 1 M HCl and 1 M NaOH solutions, and the study was conducted with an initial dye concentration of 50 mg/L, contact time of 60 min and at a temperature of 20 °C at a stirrer speed of 180 rpm. The adsorption data of PANI in Fig. 9a show that greater removal of AG25 dye was observed at lower pH values. The maximum adsorption of AG25 dye was obtained at pH = 2 (100% removal within 10 min), and the minimum adsorption was observed at pH = 8 (97.32%). The adsorption of AG25 dye was stable after a short interval time (15 min). In Fig. 9a, it can be seen that there is no significant difference in adsorption between pH 2 (100%), pH 4 (99.88%) and pH 6 (98.33%), and so pH 6 was selected as an optimum pH for the adsorption study of AG25 dye. For PANI/MMT (Fig. 9b), the maximum removal of AG25 dye was obtained at pH = 6 (100%) and the minimum adsorption was observed at pH = 10 (98.06%).

Effect of adsorbent dose

The effect of adsorbent dose was also studied for pure PANI and PANI/MMT for AG25 dye adsorption by taking various amounts of adsorbent (0.08 to 0.6 g) with an initial dye concentration of 50 mg/L at 20 °C for 60 min. The data of the effect of adsorbent are plotted between time vs percentage removal and are displayed in Fig. 10. After the dose of 0.4 g, there is hardly any difference in % removal for higher amounts (Table 4). Hence, in order to use the lowest adsorbent amount, an adsorbent amount of 0.4 g was selected for further adsorption study of AG25 dye. The percentage removal of AG25 dye increased with an increase in adsorbent amount, and this is mainly due to the availability of more active sites of the adsorbent which can interact with the solution of the anionic dye [65, 87, 88].

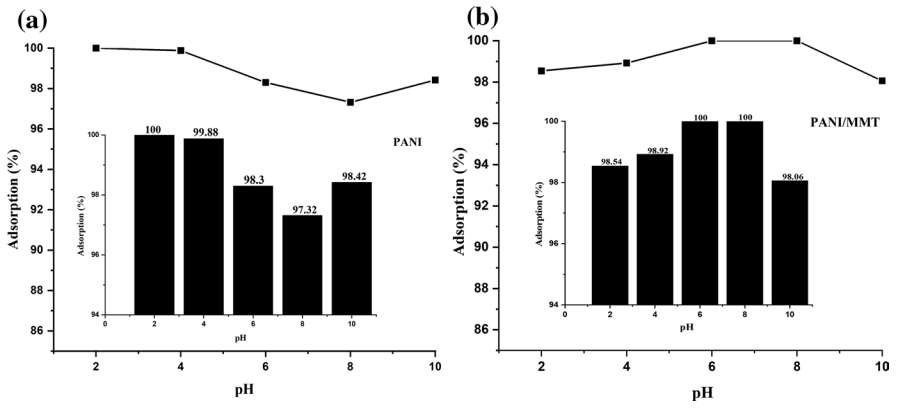

Fig. 9 Effect of pH on the removal of AG25 dye

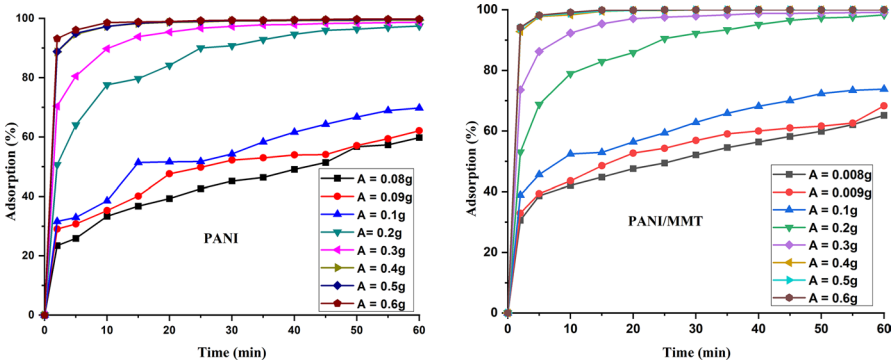

Fig. 10 Effect of adsorbent amount (pH = 6, C_o = 50 mg/L, T = 20 °C)

Table 4 Effect of PANI and PANI/MMT adsorbent dose

Adsorbent dose	0.08 g (%)	0.09 g (%)	0.1 g (%)	0.2 g (%)	0.3 g (%)	0.4 g (%)	0.5 g (%)	0.6 g (%)
% removal (PANI)	59.76	62.08	69.76	97.44	98.66	99.4	99.64	99.76
% removal (PANI/MMT)	65.14	68.3	73.8	98.3	99.16	100	100	100

Effect of initial dye concentration

The effect of initial dye concentration of AG25 dye with PANI and PANI/MMT nanocomposite adsorbents was studied. The C_o values were varied from 50 to 200 mg/L at a temperature of 20 °C, optimized pH 6 and adsorbent amount of 0.4 g. Figure 11a, b illustrates the effect of initial dye concentration on the adsorption of PANI and PANI/MMT samples. Adsorption kinetics have been compared for pure PANI and PANI/MMT at an initial dye concentration of 50 mg/L, in Fig. 11c. Pure PANI removed 94.64% and PANI/MMT removed 97.82% of the dye within 5 min at an initial dye concentration of 50 mg/L. Also, within 30 min the PANI/MMT sample removed 100% and pure PANI salt sample removed 99.16% of the anionic dye (C_o = 50 mg/L, pH = 6, adsorbent = 0.4 g, T = 2 0 °C). Since the adsorption occurs at a very fast rate, i.e., in a very short time period, the same data were plotted on a semi-log figure (the inset in Fig. 11c to illustrate the adsorption behavior at short times. It can be seen that even at 1 min, the adsorption for PANI and PANI/MMT is about 88% and 93%, respectively.

The results indicate that the efficiency of PANI/MMT nanocomposite as an adsorbent is higher as compared to that of pure PANI. On comparison of adsorption behavior at different initial dye concentration, it can be seen that the adsorption capacity of samples decreased by increasing the AG25 dye concentration.

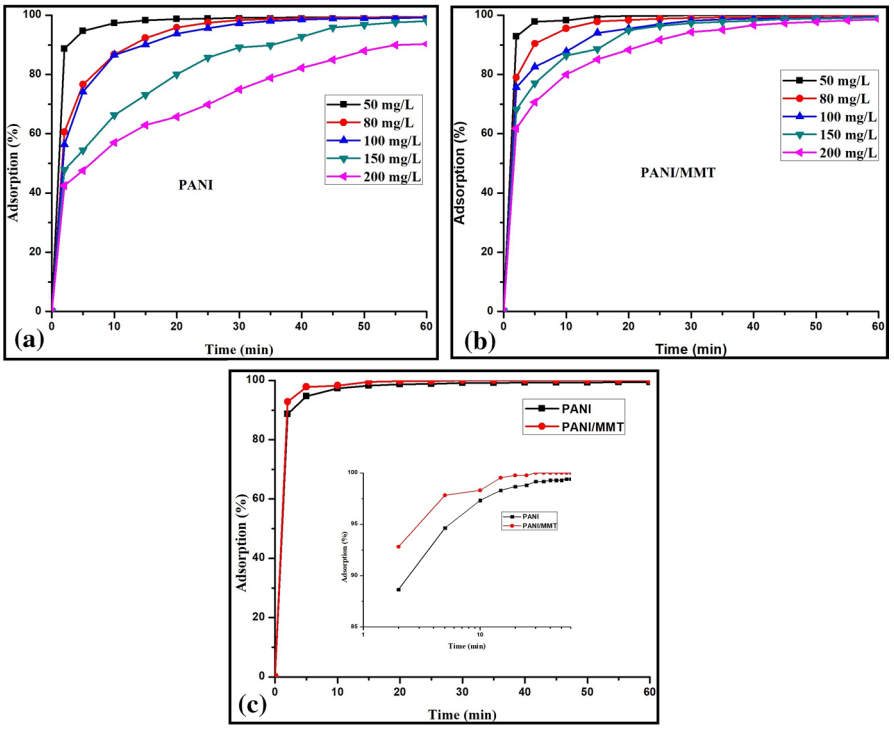

Fig. 11 Effect of initial dye concentration on AG25 dye removal by **a** PANI, **b** PANI/MMT adsorbent (T = 20 °C, pH = 6, C_o = 50–200 mg/L, t = 60 min), **c** is the comparison of PANI and PANI/MMT adsorption data (50 mg/L)

This may be attributed to the saturation of the adsorbent sites for removal the dye molecules [88, 89].

Effect of temperature

The effect of temperature was also studied for the removal of AG25 dye at 20°, 35°, 45° and 50 °C (conditions: C_o = 50–200 mg/L, pH = 6, adsorbent = 0.4 g, t = 30 min). The effect of temperature on adsorption by PANI and PANI/MMT for AG25 dye removal is shown in Fig. 12. The results indicate that the percentage removal by PANI is less than the removal by PANI/MMT nanocomposite, and removal of AG25 dye increases with an increase in temperature of the dye solution, from 20° to 50 °C [90]. The higher adsorption by the nanocomposite is due to the nanodispersed clay platelets, the outer layer of which has a negative charge.

Adsorption kinetics

There are different models available to evaluate the adsorption kinetic data. The adsorption kinetics study of AG25 dye was done using a pseudo-first-order kinetic

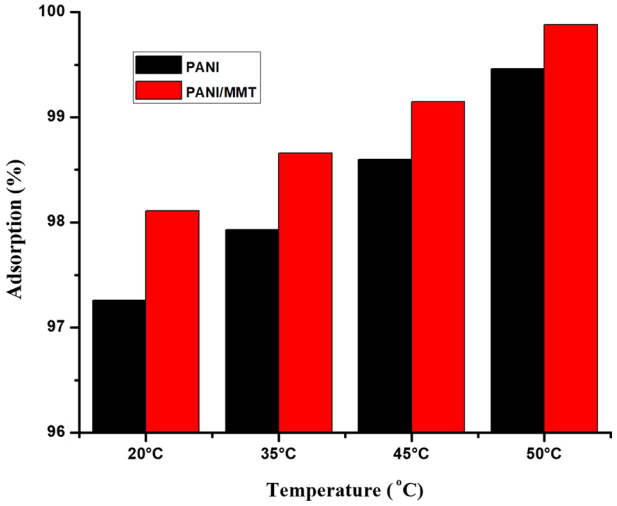

Fig. 12 Comparison of PANI with PANI/MMT adsorption for AG25 dye removal (C_o = 50 mg/L, adsorbent dose = 0.4 g, pH = 6, t = 30 min)

model as well as a pseudo-second-order kinetic model. The equation for the pseudo-first-order model can be written as [1]:

$$\log\left(q_e - q_t\right) = \log q_e - k_f t/2.303 \tag{3}$$

where q_e (mg/g) = amount of dye adsorbed at equilibrium; q_t (mg/g) = amount of dye adsorbed at time t; k_f (min^{-1}) = rate constant; t (min) = time.

The maximum adsorption time was taken to be 60 min, wherein the percentage dye removal was more than 99% for all initial dye concentration studied. The experimental data did not fit in pseudo-first-order kinetic model. First-order model is therefore not a suitable model for adsorption kinetic study of AG25 dye. Then, the pseudo-second kinetic model was tested for adsorption at different temperatures (20 to 50 °C) and different initial dye concentrations (50–200 mg/L). The equation for pseudo-second-order model can be written as [1]:

$$\frac{t}{q_t} = \frac{1}{k_2 qe^2} + \frac{t}{qe} \tag{4}$$

Where k_2 = pseudo-second-order rate constant.

The straight line (plotted between t/q_t vs. t) was obtained from pseudo-second-order kinetic model as shown in Fig. 13a, b. Tables 5 and 6 presents the pseudo-second-order kinetic parameters (q_e, k_2) calculated for AG25 dye adsorption onto PANI and PANI/MMT nanocomposite samples. The rate constant (k_2) and equilibrium adsorption capacity (q_e) values were calculated from the intercept and the slope. In the kinetic adsorption study, it was observed that the rate constant (k_2) and equilibrium adsorption capacity (q_e) values were higher for PANI/MMT nanocomposites as compared to pure PANI. These calculated k_2 values were decreased with increasing

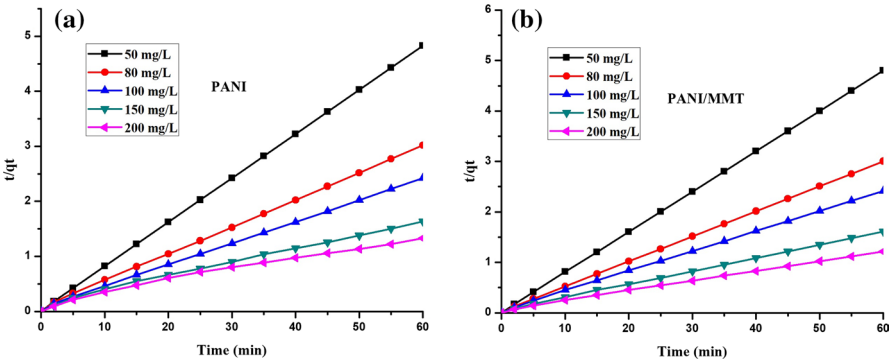

Fig. 13 Kinetics of pseudo-second-order model for adsorption of AG25 dye at 20 °C onto **a** PANI and **b** PANI/MMT

Table 5 Pseudo-second-order kinetic parameters calculated for AG25 dye adsorption on PANI

C_o (mg/L)	q_e (mg/g)	q_e (mg/g)	k_2 (g/mg min)	R^2
Temperature (T = 20 °C)				
50	12.425	12.46	0.417	0.9999
80	19.88	20.28	0.043	0.9995
100	24.78	25.37	0.028	0.9994
150	36.75	38.53	0.0066	0.9928
200	45.12	47.43	0.0038	0.9813
Temperature (T = 35 °C)				
50	12.48	12.49	1.25	1
80	19.95	20.28	0.052	0.9996
100	24.86	25.34	0.034	0.9996
150	37.28	38.77	0.0074	0.9942
200	46.70	48.56	0.0040	0.9845
Temperature (T = 45 °C)				
50	12.48	12.49	2.08	1
80	19.99	20.30	0.060	0.9996
100	24.94	25.40	0.039	0.9996
150	37.31	38.65	0.0087	0.9958
200	48.26	49.97	0.005	0.9913
Temperature (T = 50 °C)				
50	12.5	12.50	4.57	1
80	19.98	20.05	0.256	0.9999
100	24.97	25.13	0.109	0.9999
150	37.45	38.02	0.030	0.9997
200	49.49	50.89	0.009	0.9977

Table 6 Pseudo-second-order kinetic parameters calculated for AG25 dye adsorption on PANI/MMT

C_o (mg/L)	q_e (mg/g)	q_e (mg/g)	k_2 (g/mg min)	R^2
Temperature (T = 20 °C)				
50	12.5	12.52	0.79	0.9999
80	19.97	20.09	0.11	0.9999
100	24.88	25.17	0.047	0.9997
150	37.24	37.90	0.022	0.9994
200	49.30	50.50	0.010	0.9985
Temperature (T = 35 °C)				
50	12.5	12.51	1.64	1
80	20	20.10	0.160	0.9999
100	24.92	25.05	0.085	0.9999
150	37.31	37.85	0.030	0.9997
200	49.69	50.91	0.012	0.9990
Temperature (T = 45 °C)				
50	12.5	12.5	5.16	1
80	20	20.04	0.517	0.9999
100	25	25.20	0.080	0.9999
150	37.36	37.87	0.035	0.9997
200	49.78	50.89	0.014	0.9994
Temperature (T = 50 °C)				
50	12.5	12.5	5.161	1
80	20	20.04	0.567	0.9999
100	25	25.15	0.132	0.9999
150	37.47	37.95	0.040	0.9998
200	49.83	50.86	0.017	0.9995

AG25 initial dye concentration for both adsorbents (PANI and PANI/MMT). With an increase in temperature, the values of rate constant (k_2) and equilibrium adsorption capacity (q_e) were increased. It shows that the higher temperature was more efficient for AG25 adsorption onto PANI and PANI/MMT samples. High correlation coefficients ($R^2 \geq 0.99$) were obtained at 35°, 45° and 50 °C, for different initial dye concentrations. It confirms that pseudo-order model is an appropriate model to describe AG25 dye kinetic adsorption using PANI as well as PANI/MMT.

Adsorption equilibrium

An adsorption isotherm study was performed for AG25 dye with Langmuir, Freundlich and Temkin isotherm models [91]. The parameters of these three models were studied at 20°, 35° and 45 °C with the initial dye concentration range of 80–200 mg/L. Almost 100% removal was attained at all values of initial dye concentrations studied. Also, significantly the lower concentration takes very less time to achieve complete dye removal. Table 7 gives the isotherm equations for different models [1, 68, 92].

Table 7 Equations of Langmuir, Freundlich and Temkin isotherm models [1, 68, 92]

S. no	Isotherm model	Equations
1	Langmuir	$q_e = q_m K_L C_e / (1 + K_L C_e)$
2	Freundlich	$q_e = K_F C_e^{1/n}$
3	Temkin	$q_e = B_T \ln K_T + B_T \ln C_e$

Where q_e mg/g) is the adsorbate adsorbed at equilibrium, q_m is the adsorption capacity, C_e (mg/L) is the equilibrium dye concentration, K_L (L/mg) is the Langmuir isotherm constant, K_F (mg/g) and *1/n* are the Freundlich isotherm constants, and B_T (Kj/mol) and K_T (L/mg) are the Temkin isotherm constants. Out of these models, Langmuir isotherm model best fits the experimental data, as can be observed from Table 8a, b. A linear plot of C_e/q_t against C_e for AG25 dye adsorption by PANI and PANI//MMT nanocomposites was obtained as depicted in Fig. 14a, b. The highest value of correlation coefficient (R^2) for Langmuir isotherm was found in a linear plot of C_e/q_e vs C_e (Table 8a, b).

The surface area of PANI is more than that of PANI/clay nanocomposites as evidence by the BET results shown in Table 3. However, the kinetic and equilibrium adsorption data show that PANI/clay nanocomposites have higher adsorption than PANI. This is due to the fact that the outer surface of clay platelets, which are permanently negatively charged, would also adsorb the positively charged AG25 dye molecules. This is significant because the clay platelets are nanodispersed throughout the adsorbent.

Conclusion

PANI and PANI–MMT clay nanocomposites were obtained by *in situ* polymerization using ammonium persulfate as an oxidizing agent. It was observed that higher yields are obtained at the lower polymerization temperature, i.e., 0 °C, in less time. The intercalated structure of PANI/MMT nanocomposites was confirmed by HRTEM analysis. PANI and PANI/MMT nanocomposites are excellent adsorbents for anionic dye (AG25) adsorption. The dye removal is mainly dependent on the initial dye concentration, temperature and adsorbent amount. Nearly 100% removal of AG25 dye is achieved in 30 min at $C_o = 50$ mg/L, pH = 6, adsorbent = 0.4 g, $T = 20$ °C. At higher temperatures, i.e., 45 °C and 50 °C, the PANI/MMT removed 100% dye within 10 min of contact time. The adsorption of AG25 dye is higher with PANI/MMT nanocomposite and takes less time to remove 100% as compared to PANI sample. The adsorption kinetics is best described by pseudo-second-order model. The adsorption thermodynamic characteristics are best described by the Langmuir model. Overall, the study reports that PANI/MMT nanocomposite is an efficient adsorbent for AG25 textile dye adsorption and is a better adsorbent then PANI. This would be important in applications wherein they are an immobilized

Table 8 Calculated parameters for AG25 dye adsorption onto **a** PANI and **b** PANI/MMT nanocomposites

(a)			
T (°C)	q_m (mg/g)	K_L (L/mg)	R^2
Langmuir isotherm			
20	34.14	0.335	0.9993
35	36.08	0.505	0.9992
45	41.71	0.366	0.9996
T (°C)	*1/n*	K_F (mg/g)	R^2
Freundlich isotherm			
20	0.1735	3.35	0.9497
35	0.1887	3.45	0.9352
45	0.2346	3.43	0.9514
T (°C)	K_T (L/mg)	B_T (Kj/mol)	R^2
Temkin isotherm			
20	0.25	4.46	0.9790
35	0.22	5.10	0.8120
45	0.09	6.69	0.9794
(b)			
T (°C)	q_m (mg/g)	K_L (L/mg)	R^2
Langmuir isotherm			
20	51.02	0.271	0.9820
35	50.50	0.536	0.9909
45	49.87	0.969	0.9688
T (°C)	*1/n*	K_F (mg/g)	R^2
Freundlich isotherm			
20	0.3285	3.34	0.8999
35	0.2853	3.73	0.9869
45	0.1533	4.27	0.7624
T (°C)	K_T (L/mg)	B_T (Kj/mol)	R^2
Temkin isotherm			
20	0.03	9.92	0.9002
35	0.1	8.80	0.9692
45	0.06	4.65	0.6659

phase in a continuous adsorption process. Also PANI and its nanocomposites have been extensively researched for its conducting properties.

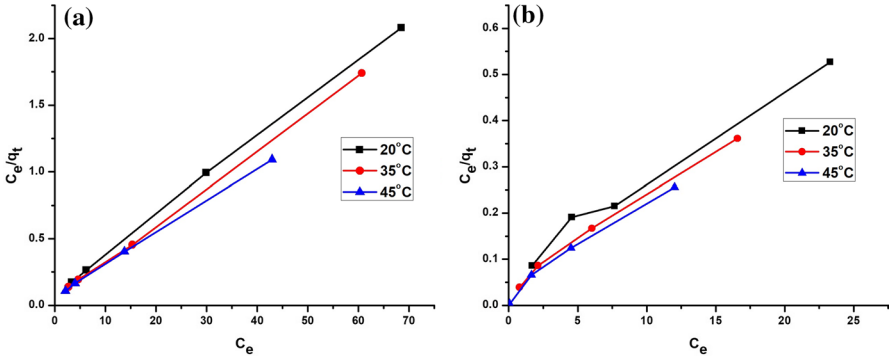

Fig. 14 Ce/qe vs Ce Langmuir plot for **a** PANI and **b** PANI/MMT (adsorbent = 0.4 g, Co = 80–200 mg/L)

Acknowledgements We would like to acknowledge the financial support from UGC (Rajiv Gandhi National Fellowship). We are also thankful to Prof S. N. Upadhyay, Emeritus Professor, Department of Chemical Engineering and Technology, IIT (BHU), for his valuable support.

References

1. Koswojo R, Utomo RP, Ju YH, Ayucitra A, Soetaredjo FE, Sunarso J, Ismadji S (2010) Acid Green 25 removal from wastewater by organo-bentonite from Pacitan. Appl Clay Sci 48:81–86
2. Salahuddin NA, Ayad MM, Essa ME (2015) Modified chitosan for efficient dye adsorption in low acid media. Int J Mater Chem 5(3):54–63. https://doi.org/10.5923/j.ijmc.20150503.02
3. Ayad MM, El-Nasr AA (2012) Anionic dye (acid green 25) adsorption from water by using polyaniline nanotubes salt/silica composite. J Nanostructure Chem 3:3
4. Ansari R, Alaei S, Mohammad-khah A (2011) Application of polyaniline for removal of acid green 25 from aqueous solution. J Sci Ind Res 70(9):804–809
5. Khan MI, Ansari TM, Zafar S, Buzdar AR, Khan MA, Mumtaz F, Prapamonthon P, Akhtar M (2018) Acid Green-25 removal from wastewater by anion exchange membrane: adsorption kinetic and thermodynamic studies. Membr Water Treat 9(2):79–85
6. Lee SY, Shim HE, Yang JE, Choi YJ, Jeon J (2019) Continuous flow removal of anionic dyes in water by chitosan-functionalized iron oxide nanoparticles incorporated in a dextran gel column. Nanometer 9:1164. https://doi.org/10.3390/nano9081164
7. Kaykhaii M, Sasani M, Marghzari S (2018) Removal of Dyes from the environment by adsorption process. Chem Mater Eng 6(2):31–35. https://doi.org/10.13189/cme.2018.060201
8. Jain SN, Gogate PR (2018) Efficient removal of Acid Green 25 dye from wastewater using activated Prunus Dulcis as biosorbent: batch and column studies. J Environ Manag 210:226–238
9. Mahmoodi NM, Taghizadeh M, Taghizadeh A (2019) Activated carbon/metal-organic framework composite as a bio-based novel green adsorbent: preparation and mathematical pollutant removal modeling. J Mol Liq 277:310–322
10. Cottet L, Almeida CAP, Naidek N, Viante MF, Lopes MC, Debacher NA (2014) Adsorption characteristics of montmorillonite clay modified with iron oxide with respect to methylene blue in aqueous media. Appl Clay Sci 95:25–31
11. Yap PW, Priyaa V (2019) Removal of crystal violet and acid green 25 from water using kaolin. Mater Sci Eng 495:012052. https://doi.org/10.1088/1757-899X/495/1/012052
12. Unuabonah EI, Taubert A (2014) Clay–polymer nanocomposites (CPNs): Adsorbents of the future for water treatment. Appl Clay Sci 99:83–92
13. Olad A, Rashidzadeh A (2012) Poly(N-vinylpyrrolidone) modified polyaniline/Na+ -cloisite nanocomposite: synthesis and characterization. Fiber Polym 13:16–20

14. Mahanta D, Madras G, Radhakrishnan S, Patil S (2008) Adsorption of sulfonated dyes by polyaniline emeraldine salt and its kinetics. J Phys Chem 112:10153–10157
15. Souza FG, Sirelli L, Michel RC, Soares BG, Herbst MH (2006) In situ polymerization of aniline in the presence of carbon black. J Appl Polym Sci 102:535–541
16. Palaniappan S, John A (2008) Polyaniline materials by emulsion polymerization pathway. Prog Polym Sci 33:732–758
17. Baei MS, Babaee V, Pirouz F (2011) Preparation of polyaniline nanocomposites for removal of sulfate from wastewater. In: 2nd International conference on chemistry and chemical engineering vol 14, p 95
18. Chowdhury AN, Jesmeen SR, Hossain MM (2004) Removal of dyes from water by conducting polymeric adsorbent. Polym Adv Technol 15:633–638
19. Chen CH (2003) Thermal and morphological studies of chemically prepared emeraldine-base-form polyaniline powder. J Appl Polym Sci 89:2142–2148
20. Zahran M, Saleeb MM, Elhalawany N (2019) Electrical and dielectrical properties of some novel polyaniline nanocomposites. Egypt J Chem 62(11):1987–1994
21. Salem MA (2010) The role of polyaniline salts in the removal of direct blue 78 from aqueous solution: a kinetic study. React Funct Polym 70:707–714
22. Elsayed AH, Mohy Eldin MS, Elsyed AM, Abo Elazm AH, Younes EM, Motaweh HA (2011) Synthesis and properties of polyaniline/ferrites nanocomposites. Int J Electrochem Sci 6:206–221
23. Boddula R, Srinivasan P (2014) Emeraldine Base form of polyaniline nanofibers as new, economical, green, and efficient catalyst for synthesis of Z-Aldoximes. J Catal. https://doi.org/10.1155/2014/515428
24. Yeh JM, Liou SJ, Lai CY, Wu PC (2001) Enhancement of corrosion protection effect in polyaniline via the formation of polyaniline-clay nanocomposite Materials. Chem Mater 13:1131–1136
25. Stejskal J, Gilbert RG (2002) Polyaniline, preparation of a conducting polymer. Pure Appl Chem 74:857–867
26. Palaniappan S, John A, Amarnath CA, Rao VJ (2004) Mannich-type reaction in solvent free condition using reusable polyaniline catalyst. J Mol Catal A: Chem 218:47–53
27. Ramamurthy PC, Harrell WR, Gregory RV, Sadanadan B, Rao AM (2004) mechanical and electrical properties of solution-processed polyaniline multiwalled carbon nanotube composite films. J Electrochem Soc 151:502–506
28. Acevedo DF, Salavagione HJ, Miras MC, Barbero CA (2005) Synthesis, properties and aplications of functionalized polyanilines. J Braz Chem Soc. https://doi.org/10.1590/S010350532005000200020
29. Ansari R (2006) Application of polyaniline and its composites for adsorption/recovery of chromium (VI) from aqueous solutions. Acta Chim Slov 53(1):88–94
30. Chang KC, Jang GW, Peng CW, Lin CY, Shieh JC, Yeh JM, Yang JC, Li WT (2007) Comparatively electrochemical studies at different operational temperatures for the effect of nanoclay platelets on the anticorrosion efficiency of DBSA-doped polyaniline/Na+–MMT clay nanocomposite coatings. Electrochim Acta 52:5191–5200
31. Simoes FR, Bulhoes LOS, Pereira EC (2009) Synthesis and characterization of conducting composites of polyaniline and carbon black with high thermal stability. Polimeros 19:54–57
32. Babazadeh M (2009) Aqueous dispersions of DBSA-doped polyaniline: one-pot preparation, characterization, and properties study. J Appl Polym Sci 113:3980–3984
33. Chauhan NPS, Ameta R, Ameta R, Ameta SC (2011) Thermal and conducting behaviour of emeraldine base (EB) form of polyaniline (PANI). Indian J Chem Technol 18(2):118–122
34. Pande S, Swaruparani H, Bedre MD, Bhat R, Deshpande R, Venkataraman A (2012) Synthesis, characterization and studies of PANI–MMT nanocompoisites. Nanosci Nanotechnol 2:90–98
35. Kavitha B, Siva Kumar K, Narsimlu N (2013) Synthesis and characterization of polyaniline nanofibers. Indian J Pure Ap Phy 51(3):207–209
36. Wasu MB, Raut AR (2014) Synthesis and characterization of polyaniline based conducting polymers. J Chem Cheml Sci 4(2):90–97
37. Sharma D, Kaith BS, Rajput J (2014) Single step in situ synthesis and optical properties of polyaniline/ZnO nanocomposites. Sci World J. https://doi.org/10.1155/2014/904513
38. Sangamesha MA, Pushpalatha K, Shekar GL (2014) Synthesis and characterization of conducting polyaniline/copper selenide nanocomposites. Indian J Adv Chem Sci 2(3):223–227

39. Najim TS, Salim AJ (2017) Polyaniline nanofibers and nanocomposites: Preparation, characterization, and application for Cr(VI) and phosphate ions removal from aqueous solution. Arab J Chem 10:S3459–S3467. https://doi.org/10.1016/j.arabjc.2014.02.008
40. Bavio MA, Acosta GG, Kessler T (2014) Polyaniline and polyaniline-carbon black nanostructures as electrochemical capacitor electrode materials. Int J Hydrog Energy 39:8582–8589
41. Kim BH, Jung JH, Hong SH, Joo J (2002) Nanocomposite of polyaniline and Na+-montmorillonite clay. Macromolecules 35:1419–1423
42. Nascimento GM, Constantino VRL, Landers R, Temperini MLA (2004) Aniline polymerization into montmorillonite clay: a spectroscopic investigation of the intercalated conducting polymer. Macromolecules 37:9373–9385
43. Nascimento GM, Constantino VRL, Landers R, Temperini MLA (2006) Spectroscopic characterization of polyaniline formed in the presence of montmorillonite clay. Polymer 47:6131–6139
44. Binitha NN, Sugunan S (2008) Polyaniline/pillared montmorillonite clay composite nanofibers. J Appl Polym Sci 107:3367–3372
45. Kalaivasan N, Shafi SS (2010) Synthesis of various polyaniline / clay nanocomposites derived from aniline and substituted aniline derivatives by mechanochemical intercalation method. E-J Chem 7(4):1477–1483
46. Narayanan BN, Koodathil R, Gangadharan T, Yaakob Z, Saidu FK, Chandralayam S (2010) Preparation and characterization of exfoliated polyaniline/montmorillonite nanocomposites. Mater Sci Eng B 168:242–244
47. Srivastava N, Singh Y, Singh RA (2011) Preparation of intercalated polyaniline/clay nanocomposite and its exfoliation exhibiting dendritic structure. Bull Mater Sci 34:635–638
48. Binitha N, Suraja V, Yaakob Z, Sugunan S (2011) Synthesis of polyaniline-montmorillonite nanocomposites using H_2O_2 as the oxidant. Sains Malays 40(3):215–219
49. Kazim S, Ahmad S, Pfleger J, Plestil J, Joshi YM (2011) Polyaniline–sodium montmorillonite clay nanocomposites: effect of clay concentration on thermal, structural, and electrical properties. J Mater Sci 47:420–428
50. Baldissera AF, Souza JF, Ferreira CA (2013) Synthesis of polyaniline/clay conducting nanocomposites. Synth Met 183:69–72
51. Deng S, Guang Li G (2013) structural features and microwave absorbing properties of polyaniline-montmorillonite composites prepared by in-situ. J Fiber Bioeng Informat 6(1):33–40
52. Abd El-Ghaffar MA, Youssef AM, Abd El-Hakim AA (2015) Polyaniline nanocomposites via in situ emulsion polymerization based on montmorillonite: preparation and characterization. Arab J Chem 8(6):771–779. https://doi.org/10.1016/j.arabjc.2014.01.001
53. Nguyen VH, Shim JJ (2015) Green synthesis and characterization of carbon nanotubes/polyaniline nanocomposites. J Spectrosc. https://doi.org/10.1155/2015/297804
54. Leon-Almazan CMD, Estrada-Moreno IA, Páramo-García U, Rivera-Armenta JL (2018) Polyaniline/clay nanocomposites. A comparative approach on the doping acid and the clay spacing technique. Synth Met 236:61–67
55. Yamabe K, Goto H (2018) Synthesis and surface observation of montmorillonite/polyaniline composites. J Compos Sci 2:15. https://doi.org/10.3390/jcs2010015
56. Hattab Y, Benharrats N (2019) Electrical and thermal properties of PANI–Mmt nanocomposites in strongly acidic aqueous media. SN Appl Sci 1:750. https://doi.org/10.1007/s42452-019-0703-1
57. Nigam V, Lal G (2008) Review on recent trends in polymer layered clay nanocomposites. Proc Indian Natn Sci Acad 74(2):87–96
58. Benhebal H, Chaib M, Leonard AL, Crine M, Lambert SD (2014) Preparation of polyaniline-modified local clay and study of its sorption capacity. J Nanost Chem 4:98
59. Qureshi UA, Gubbuk IH, Ersoz M, Solangi AR, Taqvi SIH, Memon SQ (2016) Preparation of polyaniline montmorillonite clay composites for the removal of diethyl hexyl phthalate from aqueous solutions. Sep Sci Technol 51(2):214–228
60. Ramedani A, Yazdanpanah A, Abrishamkar A, Nasrollahi M, Milan PB, Moghadam ZS, Chauhan NPS, Sefat F, Mozafari M (2019) Advanced characterization tools for PANI and PANI-clay nanocomposites. Fundam Emerg Appl Polyaniline. https://doi.org/10.1016/B978-0-12-817915-4.00012-9
61. Buruga K, Song H, Shang J, Bolan N, Kalathi JT, Kim K-H (2019) A review on functional polymer-clay based nanocomposite membranes for treatment of water. J Hazard Mater 379:120584. https://doi.org/10.1016/j.jhazmat.2019.04.067

62. Zeggai FZ, Belbachir M, Hachemao A (2017) In-situ preparation of conducting polymers/copper (II)-maghnite clay nanocomposites. Mat Sci Res India 14(2):204–211
63. Banimahd Keivani M, Zare K, Aghaie H, Ansari R (2009) Removal of methylene blue dye by application of polyaniline nano composite from aqueous solutions. J Phys Theor Chem 6(1):50–56
64. Rahimi R, Kerdari H, Rabbania M (2014) Adsorptive removal of crystal violet (CV), a carcinogenic textile dye, from aqueous. In: 14th International electronic conference on synthetic organic chemistry ECSOC-14
65. Ansari R, Mosayebzadeh Z (2011) Application of polyaniline as an efficient and novel adsorbent for azo dyes removal from textile wastewaters. Chem Pap 65(1):1–8
66. Janaki V, Vijayaraghavan K, Oh BT, Lee KJ, Muthuchelian K, Ramasamy AK, Kannan SK (2012) Starch/polyaniline nanocomposite for enhanced removal of reactive dyes from synthetic effluent. Carbohydr Polym 90:1437–1444
67. Baseri JR, Palanisamy PN, Sivakumar P (2012) Application of polyaniline nano composite for the adsorption of acid dye from aqueous solutions. J Chem 9(3):1266–1275
68. Ansari R, Dezhampanah H (2013) Application of polyaniline /sawdust composite for removal of acid green 25 from aqueous solutions: kinetics and thermodynamic studies. Eur Chem Bull 2(4):220–225. https://doi.org/10.17628/ecb.2013.2.220-225
69. Karthikaikumar S, Karthikeyan M, Satheesh Kumar KK (2014) Removal of congo red dye from aqueous solution by polyaniline- montmorillonite composite. Chem Sci Rev Lett 2(8):606–614
70. Olad A, Azhar FF (2014) Eco-friendly biopolymer/clay/conducting polymer nanocomposite: characterization and its application in reactive dye removal. Fiber Polym 15:1321–1329
71. Shahabuddin S, Sarih NM, Kamboh MA, Nodeh HR, Mohamad S (2016) Synthesis of polyaniline-coated graphene Oxide@SrTiO3 nanocube nanocomposites for enhanced removal of carcinogenic dyes from aqueous solution. Polymers 8(9):305
72. Khairy M, Kamal R, Amin NH, Mousa MA (2016) Kinetics and isotherm studies of Remazol Red adsorption onto polyaniline/ cerium oxide nanocomposites. J Bas Environ Sci 3:123–132
73. Gemeay AH, Elsharkawy RB, Aboelfetoh EF (2018) Graphene oxide/polyaniline/manganese oxide ternary nanocomposites, facile synthesis, characterization, and application for indigo carmine removal. J Polym Environ 26:655–669
74. Soltani H, Belmokhtar A, Zeggal FZ, Benyoucef A, Bousalem S, Bachari K (2019) Copper(II) removal from aqueous solutions by PANI-clay hybrid material: fabrication, characterization, adsorption and kinetics study. J Inorg Organomet Polym Mater 29:841–850
75. Zehhaf A, Morallon E, Benyoucef A (2013) Polyaniline/montmorillonite nanocomposites obtained by in situ intercalation and oxidative polymerization in cationic modified-clay (sodium, copper and iron). J Inorg Organomet Polym Mater 23:1485–1491
76. HambateGomdje V, Rahman AN, Wahabou A, BenoitLoura, Chtaini A (2017) Synthesis of organoclay and its applications in electrochemical detection of paracetamol. Der Chem Sin 8(1):206–217
77. Tyagi B, Chudasama CD, Jasra RV (2006) Determination of structural modification in acid activated montmorillonite clay by FT-IR spectroscopy. Spectrochim Acta A 64:273–278
78. Gomes EC, Oliveira MAS (2012) Chemical polymerization of aniline in hydrochloric acid (HCl) and formic acid (HCOOH) media. Differences between the two synthesized polyanilines. Am J Polym Sci 2:5–13
79. Cole KC (2008) Use of infrared spectroscopy to characterize clay intercalation and exfoliation in polymer nanocomposites. Macromolecules 41:834–843
80. Qiu M, Zhang Y, Wen B (2018) Facile synthesis of polyaniline nanostructures with effective electromagnetic interference shielding performance. J Mater Sci-Mater El 29:10437–10444
81. Nadaf LI, Venkatesh KS (2015) Polyaniline-copper oxide nano-composites: Synthesis and characterization. Mat Sci Res India 12(2):108–111. https://doi.org/10.13005/msri/120204
82. Sui X, Chu Y, Xing S, Liu C (2004) Synthesis of PANI/AgCl, PANI/$BaSO_4$ and PANI/TiO_2 nanocomposites in CTAB/hexanol/water reverse micelle. Mater Lett 58:1255–1259
83. Vivekanandan J, Ponnusamy V, Mahudeswaran A, Vijayanand PS (2011) Synthesis, characterization and conductivity study of polyaniline prepared by chemical oxidative and electrochemical methods. Arch Appl Sci Res 3(6):147–153
84. Jayasudha S, Priya L, Vasudevan KT (2014) Preparation and characterization of Polyaniline/Ag nanocomposites. Int J Chem Tech Res 6(3):1821–1823
85. Yoshimoto S, Ohashi F, Kameyama T (2005) Characterization and thermal degradation studies on polyaniline-intercalated montmorillonite nanocomposites prepared by a solvent-free mechanochemical route. J Polym Sci B 43:2705–2714

86. Sun F, Pan Y, Wang J, Wang Z, Hu C, Dong Q (2009) Synthesis of conducting polyaniline-montmorillonite nanocomposites via inverse emulsion polymerization in supercritical carbon dioxide. Polym Compos 31:163. https://doi.org/10.1002/pc.20783
87. Salem MA, Elsharkawy RG, Hablas MF (2016) Adsorption of brilliant green dye by polyaniline/silver nanocomposite: kinetic, equilibrium, and thermodynamic studies. Eur Polym J 75:577–590. https://doi.org/10.1016/j.eurpolymj.2015.12.027
88. Sobhanardakani S, Zandipak R (2015) Removal of anionic dyes (Direct Blue 106 and Acid Green 25) from aqueous solutions using oxidized multi-walled carbon nanotubes. Iran J Health Sci 3(3):48–57
89. Inthapanya X, Wu S, Han Z, Zeng G, Wu M, Yang C (2019) Adsorptive removal of anionic dye using calcined oyster shells: isotherms, kinetics, and thermodynamics. Environ Sci Pollut Res 6:5944–5954
90. Youssef AM, Ahmed AI, El-Bana UA (2012) Adsorption of cationic dye (MB) and anionic dye (AG 25) by physically and chemically activated carbons developed from rice husk. Carbon Lett 13(2):61–72
91. Parimalam R, Raj V, Sivakumar P (2012) Removal of acid green 25 from aqueous solution by adsorption. E-J Chem 9:1683–1698
92. Salahuddin NA, Ayad MM, Essa ME (2015) Modified chitosan for efficient dye adsorption in low acid media. J Mater Chem 5(3):54–63. https://doi.org/10.5923/j.ijmc.20150503.02